scientific reports

Check for updates

OPEN

Multi-scale influence mechanism of fine coal gangue on the mechanical properties of concrete

Dawei Hu[1,3], Deyu Lou[1], Yugen Li[1,3,5]✉, Peng He[2], Xiaoli Ma[1,3], Yuning Kang[4] & Feng Wei[1,3]

The aim of this study is to explore the feasibility of coal gangue (CG) fine aggregate replacing natural sand, and realize the resource utilization of solid waste in concrete materials. The coal gangue concrete (CGC) is prepared with the CG replacement of 0%, 5%, 10%, 15%, 20%, 50% and 100%, the influence of CG replacement on the slump, bulk density, compressive strength and pore structure of concrete is analyzed, and the influence mechanism is revealed combining with the scanning electron microscope (SEM), nuclear magnetic resonance (NMR) and X-ray diffractometer (XRD). The results shows that the optimal mechanical property is achieved with 10% CG replacement, which is 10.1% higher than that of the ordinary concrete. The influence mechanism is that it accelerates the hydration reaction of cement, improves the interfacial transition zone (ITZ), increases the harmless pores percentage and reduces the more harmful pores percentage. The research provides theoretical support for the high value utilization of solid waste in mining area.

Keywords Coal gangue fine aggregate, Compressive strength, Interfacial transition zone, Pore structure

CG is the main solid waste produced in the process of coal mining and washing, which is mainly composed of carbon-containing rocks with the high carbon content of 20%–30% and diverse rock types[1–5]. As one of the industrial solid wastes with the largest emissions[6,7], the cumulative stock of CG in China has exceeded 7 billion tons, and the annual increase continues to rise, which not only wastes land but also pollutes the environment[8–11]. At the same time, with the acceleration of urbanization, the demand for sand and gravel aggregate in the construction industry has surged, leading to a serious shortage of natural sand resources, and its annual shortage is as high as hundreds of millions of tons[12]. Therefore, it is urgent need to develop new sources of sustainable alternative sand for construction.

Although the accumulation of CG seriously restricting the green transformation of the coal industry, but its mineral composition and physical properties are similar to those of natural sand and gravel aggregates, showing great potential in the field of building materials[13–16]. In recent years, the research on CG as concrete aggregate for preparing CGC has attracted much attention[17–19]. Cheng et al[20]. the optimal content of coal gangue is between 20% and 30%, and the maximum content is 40%; Gao[21] found that the compressive strength of concrete shows a decreasing trend with the increase of CG aggregate replacement, the compressive strength of CGC reduced by 50% with the CG replacement of 100%. Zhang et al.[22] pointed out that when the CG substitution rate is 30%, the comprehensive strength of concrete reaches the optimal level. Gong[23] and Li et al.[24] also obtained similar conclusions. Meanwhile, CG can alter the ITZ structure and porosity of materials when added to make CGC owing to its physical and chemical properties, which leads to differences from ordinary concrete in terms of workability and mechanical properties. Qiu[25]found that with the replacement rates of coal gangue manufactured sand are 20% and 40% respectively, the proportion of harmful pores is reduced by 3.9% and 3.3% respectively, and the proportion of harmless pores is increased by 10.4% and 2.8% respectively. Zhou et al[26]. studied the mechanical damage and microstructure of CGC and found that the ITZ between coal gangue and cement paste is the weakest part in CGC.

Existing studies have significant guiding significance for the resource utilization of CG as sand and gravel aggregates, but limitations remain. First, there are relatively few achievements focusing on the influence of CG fine aggregates on the technical properties of concrete. Second, the microscopic mechanism of CG on the technical properties of concrete needs to be deepened. Moreover, the influence of CG from Shaanbei Mining

[1]School of Architectural Engineering, Yulin University, Yulin 719000, China. [2]Yulin High-tech Construction Engineering Quality Testing Co., LTD, Yulin 719000, Shaanxi, China. [3]Shaanxi Key Laboratory of Waste Resource Utilization and Energy Saving Building Materials in Mining Area, Yulin 719000, China. [4]Network information center, Yulin University, Yulin 719000, China. [5]Yulin University, No. 4 Chongwen Road, Yulin 719000, China. ✉email: liyugen@yulinu.edu.cn

Aggregate	Bulk density/(kg.m^{-3})	Apparent density/(kg.m^{-3})	Crushing value/%
River sand	1570	2424	23.61
CG	1460	2167	30.97

Table 1. Performance parameters of fine aggregates.

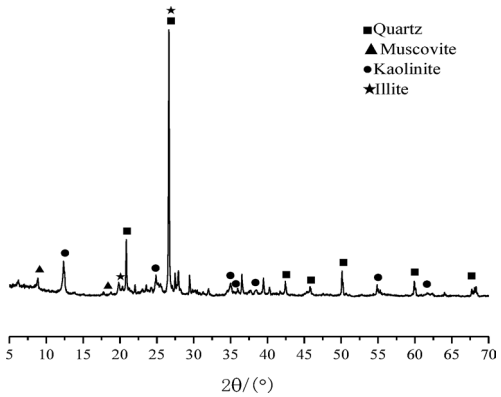

Fig. 1. CG aggregate XRD.

Area on the relevant properties of concrete requires further analysis. Furthermore, recent studies have enhanced the understanding of concrete under dynamic loading and its structural applications[27–29]. These findings provide important references for evaluating the mechanical response and failure mechanisms of CGC under dynamic conditions, offering theoretical support for seismic design and impact resistance optimization of engineering structures in mining areas. However, there is still a lack of systematic multi-scale research that correlates macroscopic mechanical properties with the evolution of the ITZ, pore structure, and phase composition, particularly for fine coal gangue aggregates from the Shaanbei region. This study aims to fill this specific gap. Thus, CGC is prepared by replacing river sand with CG from northern Shaanxi with the gradient replacement of 0%–100% to investigate the influence of CG on the workability and compressive strength of concrete, and the influence mechanism is revealed combining with SEM, NMR and XRD.

Raw materials and test methods

Materials

Both river sand and CG is used as fine aggregate in this study. The river sand is coarse sand with a fineness modulus of 3.2. The CG is gathered from Shanbei mining area of China with a fineness modulus of 2.4, and the performance parameters as shown in Table 1, the XRD spectrum as shown in Fig. 1. The coarse aggregate is graded crushed stone with the particle sizes of 5–20 mm. The cement is P·O 42.5R ordinary Portland made by Fuping Weibang Plastic Industry Co., Ltd. with the standard consistency water consumption of 26.7%, a 3 d compressive strength of 30.3 MPa and a 28 d compressive strength of 59.2 MPa, respectively; The water reducing agent is produced by Shanxi Feike New Materials Technology Co., Ltd. with a water reduction rate of 27%. To mitigate the significant difference in fineness modulus between CG (2.4) and river sand (3.2), and to ensure the consistency of the overall gradation of the blended fine aggregate (river sand + CG) under different replacement ratios, the particle size distribution of the blended fine aggregate in all mix proportions was carefully designed and adjusted to strictly follow the gradation curve shown in Fig. 2, aiming to comply with the medium sand zone (Zone II) requirements specified in the Chinese standard GB/T 14,684–2022[30]. The calculation results indicate that when the CG replacement ratio reached 100%, the cumulative sieving results of the blended aggregate fell outside Zone II, whereas at all other replacement ratios, the gradation curves of the blended fine aggregate remained within Zone II. This approach effectively ensured the uniformity and stability of the fine aggregate particle distribution for all experimental groups except the full replacement scenario, thereby providing a reliable basis for subsequent performance comparisons.

Mix proportions of concrete

The CGC with target strength of 30 MPa is prepared with the water-cement ratio of 0.48, sand ratio of 0.32 and CG replacement of 0%, 5%, 10%, 15%, 20%, 50% and 100% according to the Chinese testing code JGJ55-2019[31]. After molding, the specimens were covered with plastic film to prevent moisture loss and stored in the laboratory environment for 24 ± 2 h prior to demolding. After demolding, the specimens are cured by placing in a standard curing box (YH-40B) with the temperature of 20 ± 2 ℃ and the humidity of 95% until 3 d, 7 d and 28 d, respectively. The mix proportions of concrete as shown in Table 2, the grading curves of each group of test sands are shown in Fig. 2.

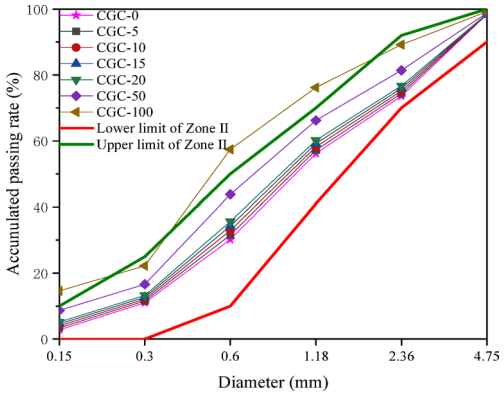

Fig. 2. Particle size distributions of sand.

Groups No.	Cement /kg.m^{-3}	Stone /kg.m^{-3}	Sand /kg.m^{-3}	Coal gangue /kg.m^{-3}	Water /kg.m^{-3}	Water reducing agent /kg.m^{-3}
RS-C	444.44	1193.78	561.78	0.00	213.33	0.00
CGC-0	444.44	1193.78	561.78	0.00	213.33	1.33
CGC-5	444.44	1193.78	533.69	28.09	213.33	1.33
CGC-10	444.44	1193.78	505.60	56.18	213.33	1.33
CGC-15	444.44	1193.78	477.51	84.27	213.33	1.33
CGC-20	444.44	1193.78	449.42	112.36	213.33	1.33
CGC-50	444.44	1193.78	280.89	280.89	213.33	1.33
CGC-100	444.44	1193.78	0.00	561.78	213.33	1.33

Table 2. Mix proportion design of CGC. Notes: RS-C-Ordinary concrete; CGC-0, CGC-5, CGC-10, CGC-15, CGC-20, CGC-50, CGC-100-CG fine aggregate concrete with the CG replacement rate of 0%,5%,10%15%,20%, 50% and 100% by equal mass.

Methods

(1) Workability and physical properties.

Water absorption The water absorption of fine aggregate is determined by a saturated surface dry conical container test mold with the size of $\Phi_{bottom} = 90$ mm, $\Phi_{top} = 40$ mm and H = 75 mm using the method of tamping 25 times with a tamping rod to determine whether it reaches the saturated surface-dry.

Bulk density The bulk density is determined by a 6-liter cylinder according to the Chinese testing code GB/T 50,080–2016[32], after vibrated with a vibrating table.

Slump The slump was measured using a slump cylinder with the size of $\Phi_{bottom} = 200$ mm, $\Phi_{top} = 100$ mm and H = 300 mm according to the Chinese testing code GB/T 50,080–2016[32], and the mixture is poured in three layers and vibrated 25 times per layer.

(2) Mechanical property.

The compressive strength test is carried out according to the Chinese testing code GB/T 50,082–2019[33] with a micro-computer electro-hydraulic pressure testing machineYAW-3000 by multiplying the conversion factor 0.95. For each mix proportion, three cube specimens were prepared and tested for compressive strength at each curing age (3 days, 7 days, and 28 days). The test data for each group satisfied the code requirement that the deviation of both the maximum and minimum values from the median value did not exceed 15%. Therefore, the compressive strength result was taken as the arithmetic mean of the three values.

(3) Microscopic characterization.

SEM characterization A cubic specimen with size of 5 mm cut from the center of CGC is used to observe the ITZ, hydration product morphology and holes of cement stone by a σ300 ffeld-emission SEM (Zeiss, Germany) with the process of immersing in anhydrous ethanol, drying and gold-plated.

NMR characterization Core samples with size of Φ50mm×100 mm are use to characterize the influence of CG on the pore structure of concrete by a Suzhou Newman MR12-150 H-I NMR (magnetic field strength 0.3 ± 0.05T, frequency 12.8 MHz) with the process of drilling from the specimens, drying at 105 °C for 24 h, pumped, and then saturated with water by immersion.

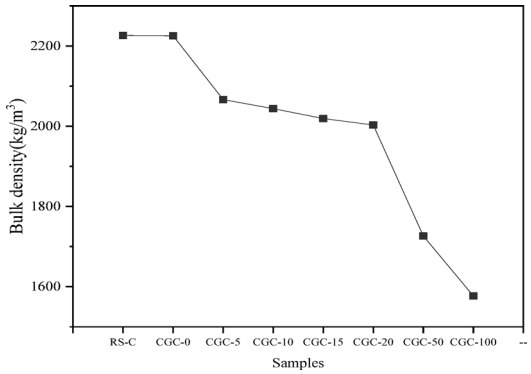

Fig. 3. The bulk densit of CGC.

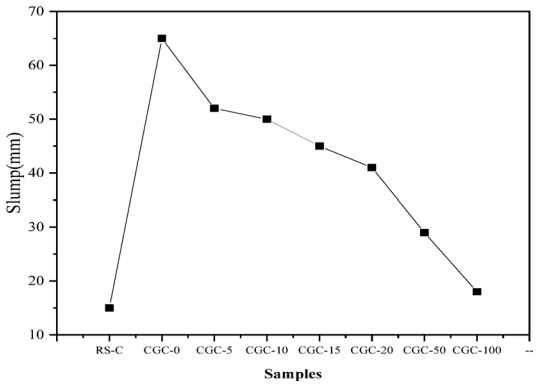

Fig. 4. The slump of CGC.

XRD characterization Cement stone diffraction samples are taken, ground with a grinder and sieved through a 200mesh sieve, and put into a Bruker D8 Advance ray diffractometer for testing.

Results and discussion

Bulk density

The relationship between bulk density of concrete and the dosage of CG is shown in Fig. 3. As can be seen that the bulk density of concrete exhibits a continuous decreasing trend as the increasing of CG dosage. The bulk density of each sample decreases by 7.1%, 8.2%, 9.3%, 10.0%, 22.4% and 29.2%, respectively, as the CG replacement increasing from 5% to 100% in comparison to CGC-0. Meanwhile, the addition of a water-reducing agent has no discernible impact on the bulk density of concrete.

The reason why CG affect the bulk density of concrete is due to its distinct physical and chemical characteristics. First, it contains higher carbon content and has light weight. Then, the structure of CG is more loose and porous than the natural river sand, which makes it light and increased voids between particles when used as aggregate[34–36] Thus, bulk density of concrete decreases as the increasing of CG addition, which is well verified by the scholar Feng[17].

Slump

The relationship between slump of concrete and the dosage of CG is shown in Fig. 4, where RS-C and CGC-0 represent the concrete with 0% CG replacement and 0% and 0.3% water reducing agent, respectively. As can be seen that the slump of CGC-0 is greatly increased by 333.3% than RS-C, that is, the addition of water-reducing agent can significantly improve the flow of concrete. Moreover, the slump of concrete decreases gradually as the increasing of CG replacement, which decreases from 65 mm (CGC-0) to 18 mm (a reduction of 72.3%) as the CG replacement increasing to 100%.

The effect of CG on the slump of concrete is due to its high water absorption properties and rich micro-porous structure of particle surface, which both clearly improve the micro-structure of ITZ between the CG and cement matrix. Furthermore, there is a large amount of dust attached to the surface of CG particles during the crushing process, which has a negative impact on the workability of concrete and leads to the decline of slump[37,38].

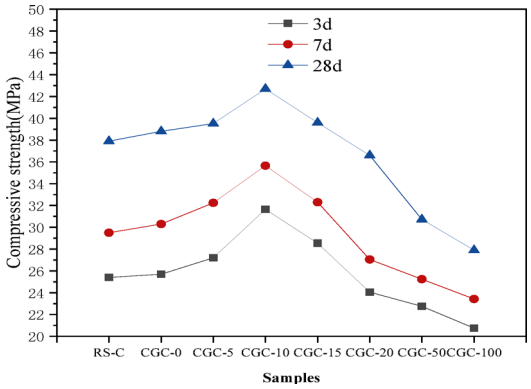

Fig. 5. The compressive strength of CGC.

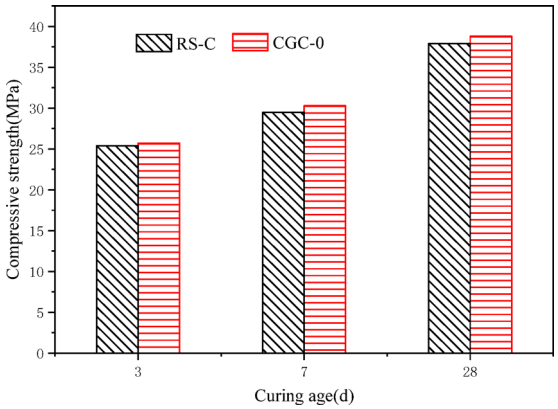

Fig. 6. The effect of water reducing agent on compressive strength.

Compressive strength

Compressive strength is one of the most indexes to evaluate the mechanical properties of concrete. Figure 5 shows the relationship between the compressive strength of concrete and CG replacement with the water reducing agent addition of 0.3%. It is easy to see that the compressive strength of concrete first increases and then decreases with the increasing of CG replacement, and the maximum strength appears at the CG replacement of 10%, which is 23.2%, 18.2% and 10.1% higher than that of CGC-0 at 3 d, 7 d and 28 d, respectively. Further analysis shows that the strength of concrete increases by 1.9%, 10.1%, 2.1%, −5.7%, −20.8% and −28.1% than CGC-0 as the CG replacement increasing from 5% to 100%.

It can also be seen from Fig. 5 that the strength of concrete shows a continuous growth with the increase of curing age. Taking the CGC-10 specimen as an example, its strength increases by 12.6% and 35.0% than that of 3 d at the curing ages of 7 d and 28 d, respectively; while the strength of CGC-100 specimen increases by 12.8% and 34.5%, respectively compared with 3 d. The reason is that more hydration products are generated with the increase of hydration reaction (the longer the curing age, the more adequate the hydration reaction), which filled the internal voids of the concrete, thereby improves the compactness.

Figure 6 shows the relationship between water reducing agent and compressive strength of concrete. It can be seen that the addition of water-reducing agent has no obvious effect on the compressive strength of concrete. Compared with RS-C, the compressive strength of CGC-0 at 3 d, 7 d and 28 d only increases by 1.1%, 2.7% and 2.3%, respectively.

Mechanism of CG on the physical and mechanical properties of concrete

Changed the water absorption characteristics of raw materials

The water absorption capacity of aggregate significantly affects the physical and mechanical properties of concrete. Test results show that the water absorption rate of river sand is 5.49%, and that of CG is 11.59%, which is significantly higher than that of river sand. The reason is that the internal porosity of CG is large, which may lead to a large slump loss of the concrete mixture in the stirring process, thereby affecting its workability.

Meanwhile, CG can reduce the effective water-cement ratio of ITZ between the cement paste and fine aggregate dues to its high water absorption rate, improve the compactness of cement paste around the CG, thereby increasing the compressive strength of concrete with the low addition of CG (no more than 15%), especially when the CG replacement is 10%, the strength of concrete reaches 42.7 MPa at 28 d, which is significantly

higher than that of CGC-0. However, it decreases the strength of concrete as the content of CG exceeds 20%. The reason is that the water consumption is insufficient and the hydration reaction of cement is insufficient when the replacement of CG is to much dues to its high water absorption rate. Moreover, the crushing value of CG is higher than that of river sand as shown in Table 1, which also results in the decrease of concrete strength.

Changed ITZ structure and morphology of hydration products

ITZ is a weak structure within concrete, which is characterized by porosity, hydrated crystallization enrichment of AFt and $Ca(OH)_2$, as well as preferred orientation, and is very important for the analysis of concrete microstructure[39–46] Fig. 7 displays the ITZ structure of concrete by taking the CGC-10 and CGC-0 as an example. As can be seen that addition of CG significantly affects the internal ITZ structure of concrete. Specifically, the structure is extremely dense, with tiny pores, uniform distribution and non-connectivity, the cracks are fine, and there are no obvious weak areas within the ITZ of CGC-10 as shown in Fig. 7(a) and (b). While for sample CGC-0, the structure of ITZ is loose and the bonding cracks are clearly visible.

Meanwhile, the hydration products are abundant, the needle and rod-shaped AFt crystals with fibrous C-S-H gels can be clearly observed near the ITZ of CGC-10 as shown in Fig. 7(c) and (d). The needle and rod-shaped AFt crystals are interwoven to form a network skeleton structure, which together with the fibrous C-S-H gel filling the pores constitute a dense cement stone structure. While for CGC-0, there are a large number of "aggregation" structures within ITZ. These structures are not closely combined and have poor integrity, resulting in many connected pores and developed cracks in this area, which in turn affects its macroscopic mechanical properties and is lower than that of CGC-10.

Moreover, Fig. 8 shows the hydration products and internal holes of CGC-10 and CGC-0. As can be seen from Fig. 8(a) and (b) that the hydration product of CGC-10 presents a highly dense overall structure, and no obvious cracks or pores are observed, indicating that its densification is significantly improved. The hydration products of CGC-0 are distributed in layers, with loose structure, large pores and micro-cracks, as well as poor integrity and low density. In addition, the smoothness of the gray-scale change in SEM images is closely related to the structural properties of the hydrated products, the smoother the grayscale change, the fewer the defects of the hydrated products, the better the structural densification, while the more intense the gray-scale change, the more the defects of the hydration product, and the looser the structure[47]. The variation of the gray value of the SEM image well proves the structure of the internal hydration products.

Figure 8(c)-(d) displays the internal holes of concrete by taking the CGC-10 and CGC-0 as an example. In the CGC-10 internal holes generated needle and rod-shaped AFt crystals and fibrous C-S-H gel, and needle and rod-shaped AFt crystals are interwoven to form a network skeleton structure, and interconnected with fibrous C-S-H gel to form a dense structure, which clinging to the surfaces of the pores to fill up the internal pores; The

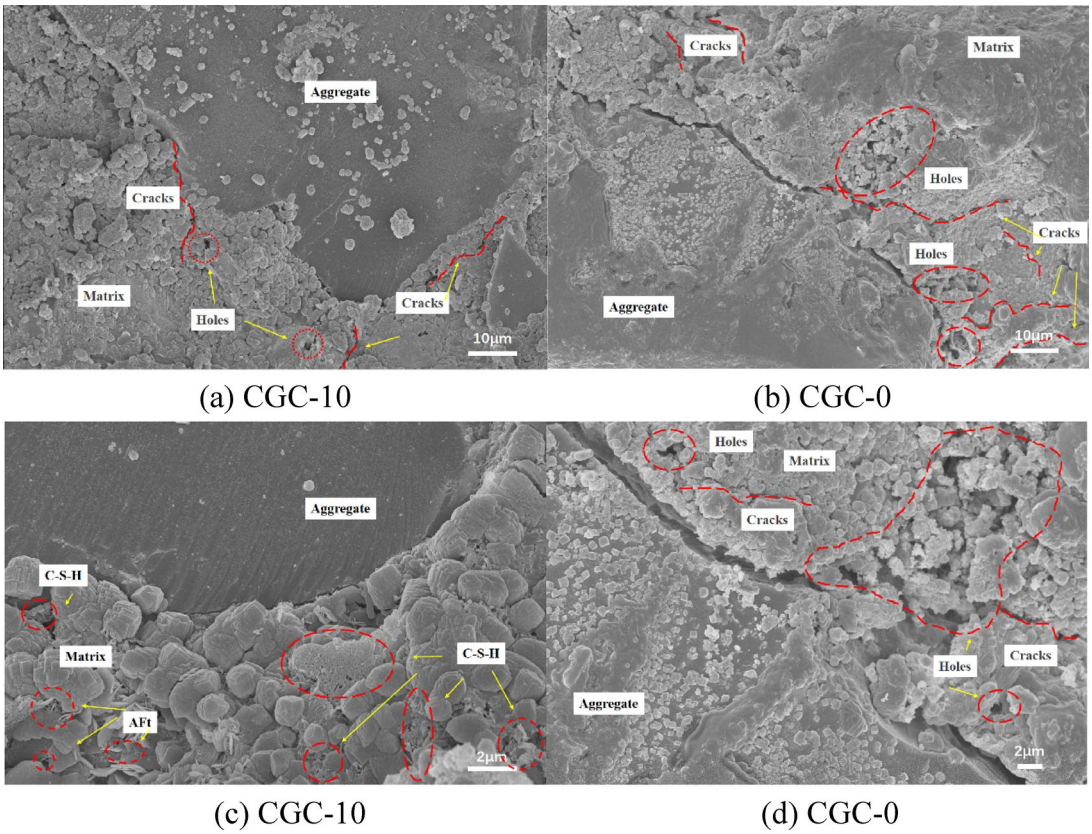

Fig. 7. ITZ structure of concrete.

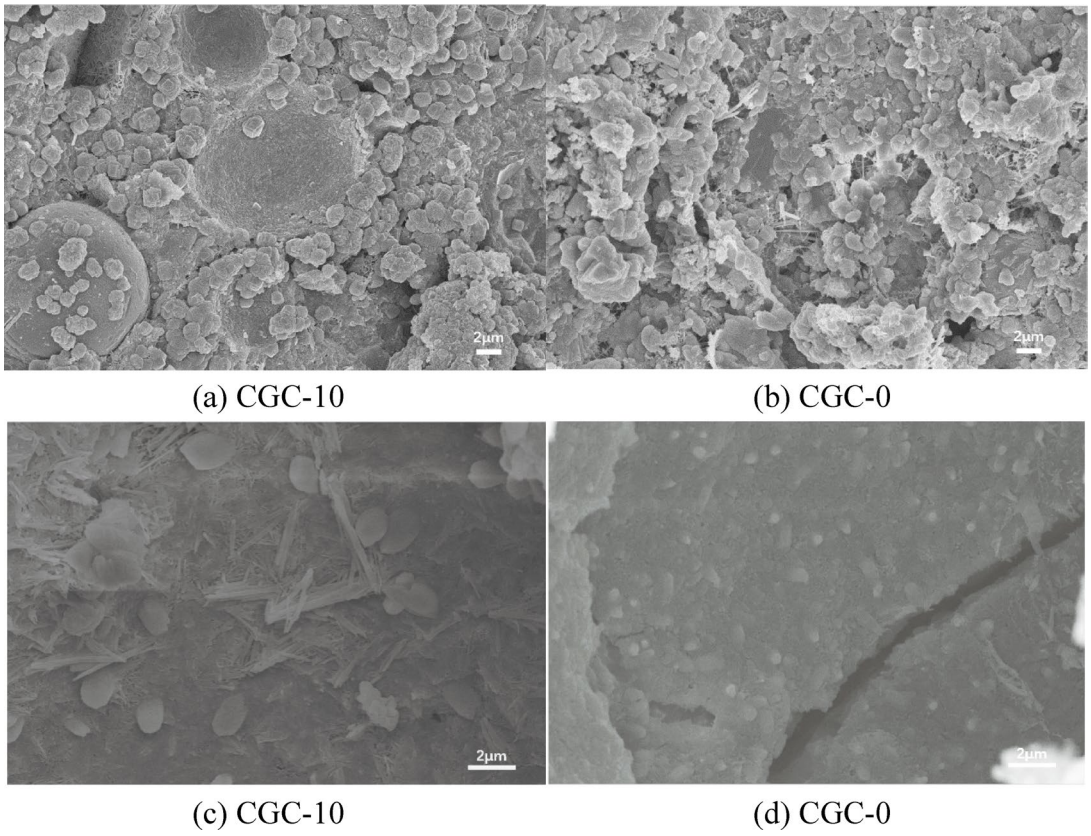

Fig. 8. Hydration products and internal holes of concrete.

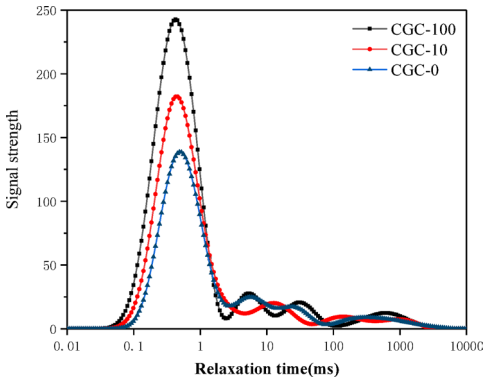

Fig. 9. T_2 spectral distribution of CGC.

hydration products inside the CGC-0 internal holes are less and there are relatively larger cracks, which have an inhibitory effect on the stability of the concrete structure.

Changed the pore structure

NMR test is an effective method to analyze the pore structure within concrete[48–52] The relationship between the transverse relaxation time (T_2) and signal intensity of CGC with the CG replacement of 0%, 10% and 100% is shown in Fig. 9 based on the NMR test. As can be seen that the peak position, intensity, width and the peak area proportion of each sample with different CG replacement is different, that is, addition of CG significantly affects the internal pore structure of concrete. For intuitive purposes, Table 3 lists the characteristic parameters of the T_2 spectra of each sample.

It can be seen that the T_2 spectral areas of CGC-0, CGC-10 and CGC-100 specimens are 4622.32, 5684.58 and 7471.69, respectively, indicating that the total area of the T_2 spectral increases with the increasing of CG replacement. Further analysis shows that the T_2 spectral areas of CGC-10 and CGC-100 increases by 22.98% and 61%, respectively compared with CGC-0.

Specimen	T_2 spectrum area	Peak 1		Peak 2		Peak 3		Peak 4	
		area	Percentage/%	area	Percentage/%	area	Percentage/%	area	Percentage/%
CGC-0	4622.32	3509.29	75.92	499.43	10.81	288.192	6.23	325.41	7.04
CGC-10	5684.58	4846.43	85.26	461.44	8.12	232.202	4.09	144.50	2.54
CGC-100	7471.69	6287.28	84.15	464.88	6.22	379.627	5.08	339.87	4.55

Table 3. NMR T_2 spectrum area.

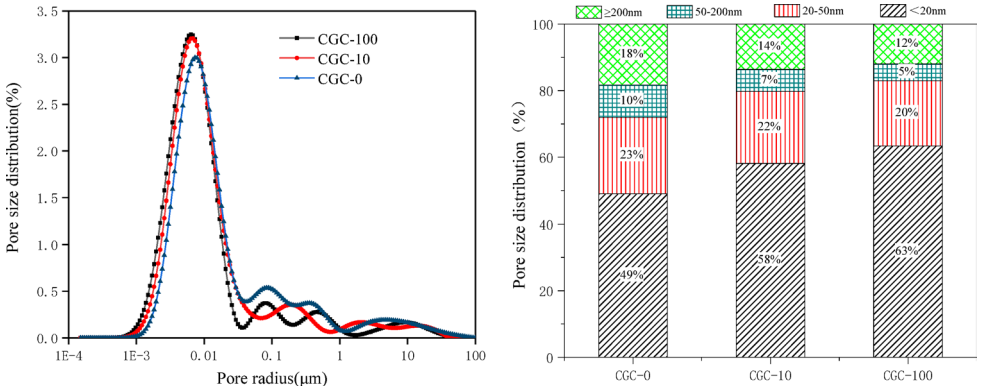

Fig. 10. Pore size distribution and pore structure of CGC.

Meanwhile, the proportion of peak 1 shows a tendency of "increasing first (75.92%→85.26%) and then decreasing (85.26%→84.148%)" as the CG replacement reaching to 100%.The proportion of peak 2 gradually decreases from 10.81% to 6.22%, while the proportion of peak 3 and peak 4 shows a tendency of "decreasing first and then increasing", which indicates that an appropriate amount of CG can improve the internal pore structure of concrete (with an increase of small pores content and a decrease of large pores content).

The reason is that it accelerates the hydration reaction of cement to generate more hydration cementitious products such as C-S-H, and increases the density of cement stone, thereby decreases the pore size.

Assuming that the pores are all ideal spheres, the total NMR relaxation rate $1/T_{2Total}$ can be expressed as:

$$\frac{1}{T_{2Total}} = \frac{1}{T_{2surface}} = \rho_2 \left(\frac{S}{V}\right)_{Pore} \tag{1}$$

$$r_c = 15T_{2Surface} \tag{2}$$

Where, ρ_2 is the surface relaxation strength, um/s, for concrete materials its value is between 3 and 10 μm/s, generally take 5 μm/s; $\left(\frac{S}{V}\right)_{Pore}$ is the pore surface area to volume ratio, um^{-1}, $\frac{S}{V} = \frac{3}{r_c}$; r_c is the pore radius, um.

Figure 10(a) shows the pore size distribution and pore ratio of each sample based on Eq. 2. It is easy to see that all samples exhibit a pore measurement range of 0.00015–150 μm, but with different peak position, intensity and width. Further analysis shows that the pore size of CGC-0 sample is mainly distributed from 0.0005 μm to 0.0274 μm (the first peak), but contains a few large holes (the maximum pore size is 86.06 μm). For the CGC-10 sample, the pore size is mainly distributed from 0.0006 μm to 37.42 μm, while the CGC-100 sample's pore size is mainly distributed from 0.0005 μm to 49.39 μm, that is, the pore size within CGC-10 is smaller than that of CGC-0 and CGC-100.

To further establish the relationship between the internal pore structure and macroscopic compressive strength of CGC, the pore structure in Fig. 10(a) is classified into harmless pores (d < 20 nm), less harmful pores (20 nm ≤ d < 50 nm), harmful pores (50 nm ≤ d < 200 nm) and more harmful pores (d ≥ 200 nm) four types in accordance with the viewpoint of academician Wu[53], and the results as shown in Fig. 10(b).

Quantitative NMR analysis of the concrete pore structure reveals that as the CG replacement ratio increases, the proportion of harmless pores increases significantly, while the proportions of harmful and more harmful pores decrease. This evolution of the pore structure is closely correlated with the enhancement of the macroscopic compressive strength. It can be seen from Fig. 10(b) that the proportion of harmless pores gradually increased from 49.02% to 63.44% as the CG replacement increasing from 0% to 100% with the speed of fast at first and then slow down. In particular, at a CG replacement ratio of 10%, the proportion of harmless pores increases from 49% (CGC-0) to 58%, representing an increase of 18.37%. Meanwhile, the proportions of the other pore types show an overall decreasing trend with increasing CG replacement: the proportion of less harmful pores decreases from 22.94% to 19.53%, harmful pores from 13.62% to 11.99%, and more harmful pores from 18.30% to 11.99%. Among these, the combined proportion of harmful and more harmful pores decreases from 28% to 21%, a reduction of 25%.

The optimization of such pore structure effectively alleviates stress concentration, improves the uniformity and compactness of the material, resulting in the 28-day compressive strength of the mixture with a CG replacement rate of 10% reaching 42.7 MPa, which is 10.1% higher than that of CGC-0. The 10% CG replacement rate has the most significant impact on the pore structure of concrete. The reason is that the active components in CG can undergo secondary hydration reactions, thereby enhancing the density of the cement stone, decreasing the pore size. Moreover, it perfects the particle gradation of the concrete aggregates, making the stones, CG, river sand and cement particles to form a continuous gradation accumulation system to reduce the pores formed by the natural accumulation of aggregates.

However, it is noteworthy that although the CGC-100 sample also exhibits a high proportion of harmless pores (63%), its total NMR T_2 spectrum area reaches 7471.69, significantly higher than those of CGC-10 (5684.58) and CGC-0 (4622.32). It indicates that under high doping amounts, although the proportion of harmless pores increases, the total number of pores rises significantly. Additionally, accompanied by the deterioration of particle gradation and insufficient moisture leading to inadequate hydration reactions, the strength ultimately decreases. Therefore, the 10% CG replacement not only optimizes pore distribution but also significantly enhances mechanical properties by maintaining a lower total pore volume. The pore structure shown in Fig. 10(b) clearly reflects the variation in concrete strength with CG replacement.

Changed phase composition

Analyzing the phase composition of hydration products is an effective means to reveal the influence mechanism of CG on the basic technical indicators of concrete from the chemical perspective[54]. Figure 11 shows the XRD patterns of concrete with different CG dosages. As can be seen that the phase composition of each sample with different CG dosages is essentially the same, but with different peak shape and peak intensity. Overall, the diffraction peaks of CGC-0 are relatively dispersed, indicating that its crystal structure is complex and may contain multiple mineral phases. However, the diffraction peak intensity of CGC-10 is relatively low, and the peak shape is relatively concentrated, that is, the crystal structure is more uniform.

The intensity of the diffraction peak corresponding to $Ca(OH)_2$ at 17.95° in CGC-10 decreased by 69% compared to CGC-0, while the diffraction peak intensities of C-S-H at 29.16°, 30.70°, 36.27°, and 49.91° increased by 215%, 315%, 220%, and 127%, respectively, relative to CGC-0. Respectively. indicating that addition of CG promotes the hydration of cement and generates more structurally stable C-S-H gel to improve the microstructure of ITZ and reduce the internal pore size within concrete as shown in Figs. 7 and 8. More specifically, the active SiO_2 and Al_2O_3 in CG (see Fig. 1 XRD peaks) react with $Ca(OH)_2$ from cement hydration (at 17.95° in Fig. 11), generating additional C-S-H gels (Fig. 7a and c), which densify the ITZ structure.

The chemical mechanism of CG to improve the mechanical properties of concrete lies in its chemical activity as shown in Fig. 12. The active SiO_2 and Al_2O_3 contained in CG undergo secondary hydration reactions with Ca^{2+} and OH^- in the cement hydration reaction system, resulting in the depolymerizing and breaking of Si-O and Al-O bonds, the forming of -Si-, -Si-OH, -Al- and -Al-OH, which will bind Ca^{2+} in the system to form more gelling products such as C-S-H and C-A-H. These products are further interwoven into a network, or even crystallized into a block or nested structure, filling in the pores inside the cement stone and the combined cracks between the paste and aggregate, thus improving the internal pore size distribution range of the concrete and the ITZ structure.

Conclusions

(1) CG can effectively replace river sand in concrete. At 10% replacement, the 28-day compressive strength reaches 42.7 MPa, exceeding the reference group by 10.1%. Concrete with 0–20% CG achieves C30 strength grade, whereas beyond 50% replacement, strength falls below C30, limiting structural applicability.

(2) The physical mechanism of CG on the strength of concrete is that it perfects the gradation of the aggregate, increases the density of concrete, improves the structure of ITZ and decreases the size of pores.

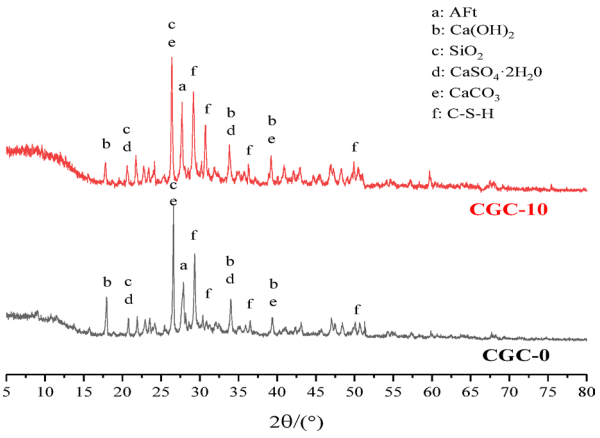

Fig. 11. XRD patterns of the cement paste in concrete.

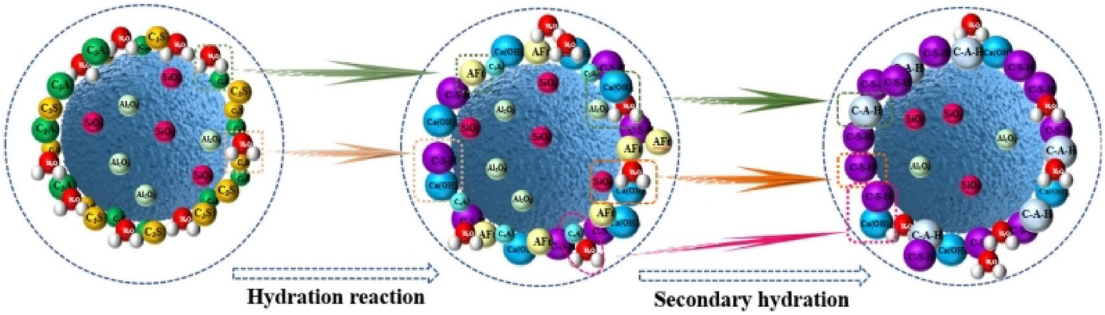

Fig. 12. Hydration process of cement.

(3) The chemical mechanism by which an appropriate amount of CG enhances the strength of concrete lies in that its chemical activity accelerates the hydration reaction of cement.

Data availability

Data is provided within the manuscript.

Received: 2 August 2025; Accepted: 15 October 2025
Published online: 31 October 2025

References

1. Li, J. Y. & Wang, J. M. Comprehensive utilization and environmental risks of coal gangue: A review. *J. Clean. Prod.* **239**, 117946. https://doi.org/10.1016/j.jclepro.2019.117946 (2019).
2. Wu, H., Wen, Q. B., Hu, L. M., Meng, G. & Tang, Z. L. Feasibility study on the application of coal gangue as landfill liner material. *Waste Manag.* **63**, 161–171. https://doi.org/10.1016/j.wasman.2017.01.016 (2017).
3. Dong, Z. C., Xia, J. W., Fan, C. & Cao, J. C. Activity of calcined coal gangue fine aggregate and its effect on the mechanical behavior of cement mortar. *Constr. Build. Mater.* **100**, 63–69. https://doi.org/10.1016/j.conbuildmat.2015.09.050 (2015).
4. Koshy, N., Dondrob, K., Hu, L. M., Wen, Q. B. & Meegoda, J. N. Synthesis and characterization of geopolymers derived from coal gangue, fly Ash and red mud. *Constr. Build. Mater.* **206**, 287–296. https://doi.org/10.1016/j.conbuildmat.2019.02.076 (2019).
5. Gao, S., Zhang, S. M. & Guo, L. H. Application of coal gangue as a coarse aggregate in green concrete production: A review. *Materials* **14** (22), 6803. https://doi.org/10.3390/ma14226803 (2021).
6. Yu, L. I. et al. Study on the mechanical behavior and micro-mechanism of concrete with coal gangue fine and coarse aggregate. *Constr. Build. Mater.* **338**, 127626. https://doi.org/10.1016/j.conbuildmat.2022.127626 (2022).
7. Yi, C. et al. Preparation and characterization of coal gangue geopolymers. *Constr. Build. Mater.* **187**, 318–326. https://doi.org/10.1016/j.conbuildmat.2018.07.220 (2018).
8. Wang, A. G. et al. Mechanism of thermal activation on granular coal gangue and its impact on the performance of cement mortars. *J. Build. Eng.* **45**, 103616. https://doi.org/10.1016/j.jobe.2021.103616 (2022).
9. Wu, B., Yu, Y., Chen, Z. P. & Zhao, X. L. Shape effect on compressive mechanical properties of compound concrete containing demolished concrete lumps. *Constr. Build. Mater.* **187**, 50–64. https://doi.org/10.1016/j.conbuildmat.2018.07.086 (2018).
10. Sun, K. K., Ali, H. A., Xuan, D. X. & Poon, C. S. Sulfuric acid resistance behaviour of alkali-activated slag and waste glass powder blended precursors. *Cem. Concr Compos.* **145**, 105319. https://doi.org/10.1016/j.cemconcomp.2023.105319 (2024).
11. Peng, B. H. et al. Bibliometric and visualized analysis of china's coal research 2000–2015. *J. Clean. Prod.* **197**, 1177–1189. https://doi.org/10.1016/j.jclepro.2018.06.283 (2018).
12. Verian, P. K., Ashraf, W. & Cao, Y. Properties of recycled concrete aggregate and their influence in new concrete production. *Resour. Conserv. Recycl.* **133**, 30–49. https://doi.org/10.1016/j.resconrec.2018.02.005 (2018).
13. Liu, Y. et al. Sustainable application of waste gangue mortar in coal mine tunnel support. *Sci. Rep.* **15**, 2682. https://doi.org/10.1038/s41598-024-81408-9 (2025).
14. Aiello, M. & Leuzzi, F. Waste tyre rubberized concrete: properties at fresh and hardened state. *Waste Manag.* **30** (8–9), 1696–1704. https://doi.org/10.1016/j.wasman.2010.02.005 (2010).
15. Guo, N., Bai, L., Yang, Y. M. & Wang, F. Feasibility study on coal based solid waste as a soil additive. *Sci. Rep.* **15**, 11068. https://doi.org/10.1038/s41598-025-88227-6 (2025).
16. Xie, S. R. et al. Technology and engineering test of filling Goaf with coal gangue slurry. *Sci. Rep.* **13**, 20536. https://doi.org/10.1038/s41598-023-47621-8 (2023).
17. Wang, Z. P., Shao, W. J., Li, H. & Cheng, S. M. Properties and hydration mechanism of cementitious materials prepared from calcined coal gangue. *J. Renew. Mater.* **11** (3), 1223–1236. https://doi.org/10.32604/jrm.2022.022893 (2022).
18. Yang, G. L. & Zha, W. H. Experimental study on the strength of coal gangue aggregate concrete with basalt fiber. *J. Phys. : Conf. Ser.* **2185** (1), 012059. https://doi.org/10.1088/1742-6596/2185/1/012059 (2022).
19. Frías, M., Rojas, D. S. M., García, R. & Valdés, A. Effect of activated coal mining wastes on the properties of blended cement. *Cem. Concr Compos.* **34** (5), 678–683. https://doi.org/10.1016/j.cemconcomp.2012.02.006 (2012).
20. Guan, H. B., Yu, J. T., Kibugenza, U., Sun, Q. W. & A.S. & Preparation of coal gangue ceramsite high-strength concrete and investigation of its physico-mechanical properties. *Sci. Rep.* **12**, 16369. https://doi.org/10.1038/s41598-022-20940-y (2022).
21. Gao, S., Zhao, G. H., Guo, L. H., Zhou, L. Q. & Yuan, K. K. Utilization of coal gangue as coarse aggregates in structural concrete. *Constr. Build. Mater.* **268**, 121212. https://doi.org/10.1016/j.conbuildmat.2020.121212 (2020).
22. Zhang, Y., Ma, G., Liu, Y. & Li, Z. Mix design for thermal insulation concrete using waste coal gangue as aggregate. *Mater. Res. Innov.* **19(sup5)**, S878–S884. https://doi.org/10.1179/1432891714Z.0000000001212 (2015).
23. Gong, P., Ma, Z. G., Ni, X. Y. & Zhang, R. R. C. An experimental investigation on the mechanical properties of gangue concrete as a roadside support body material for backfilling Gob-Side entry retaining. *Adv. Mater. Sci. Eng.* **2018** (1), 1–11. https://doi.org/10.1155/2018/1326053 (2018).
24. Li, Y. F., Liu, S. H. & Guan, X. M. Multitechnique investigation of concrete with coal gangue. *Constr. Build. Mater.* **301** (Pt.1), 124114. https://doi.org/10.1016/j.conbuildmat.2021.124114 (2021).

25. Qiu, J. S. et al. Study on Frost resistance and deterioration law of manufactured sand coal gangue concrete. *Constr. Build. Mater.* **470**, 140544. https://doi.org/10.1016/j.conbuildmat.2025.140544 (2025).
26. Zhou, M., Dou, Y. W., Zhang, Y. Z., Zhang, Y. Q. & Zhang, B. Q. Effects of the variety and content of coal gangue coarse aggregate on the mechanical properties of concrete. *Constr. Build. Mater.* **220**, 386–395. https://doi.org/10.1016/j.conbuildmat.2019.05.176 (2019).
27. Zou, S. et al. Seismic isolation effect and parametric analysis of simply supported beam bridges with multi-level sliding friction adaptive isolation bearing. *Soil. Dyn. Earthq. Eng.* **188**, 109000. https://doi.org/10.1016/j.soildyn.2024.109000 (2025).
28. Jiang, H. B. et al. Rapid hardening high performance concrete (RHHPC) for Bridge expansion joints: from material properties to interfacial shear performance. *Constr. Build. Mater.* **458**, 139638. https://doi.org/10.1016//j.conbuildmat.2024.139638 (2025).
29. Zou, S. et al. Effect of shear key geometrical dimensions on seismic performance of prefabricated concrete piers with shallow socket connections. *Structures* **71**, 107975. https://doi.org/10.1016/j.istruc.2024.107975 (2025).
30. People's Republic of China National Standard. *Construction sand(GB/T14684-2022)* (Standardization Committee of the People's Republic of China, 2022).
31. Specification for the design of normal concrete proportion(JGJ55-2019). *Ministry of Housing and* (Urban Construction of the People's Republic of China, 2019).
32. Standard for Test Methods of Performance of Normal. *Concrete Mixtures(GB/T 50080 – 2016), Published* (by China Architecture & Building, 2016).
33. Standard for Test Methods of Physical and Mechanical. *Properties of Concrete(GB/T 50081 – 2019)* (Published by China Architecture & Building, 2019).
34. Zhang, Y. L. & Dong, C. L. Reactivity activation of waste coal gangue and its impact on the properties of cement-based materials – A review. *Constr. Build. Mater.* **234**, 117424. https://doi.org/10.1016/j.conbuildmat.2019.117424 (2020).
35. Wang, Y., Zhang, X. D., Su, L. J. & Geng, J. Study on the influence of composite modified coal gangue coarse aggregate on the mechanical properties of concrete and mesoscopic simulation. *J. Build. Eng.* **106**, 112549. https://doi.org/10.1016/j.jobe.2025.112549 (2025).
36. Qiu, J. S., Zhu, M. Y., Zhou, Y. X. & Guan, X. Effect and mechanism of coal gangue concrete modification by fly Ash. *Constr. Build. Mater.* **294**, 123563. https://doi.org/10.1016/j.conbuildmat.2021.123563 (2021).
37. Mo, L. W. et al. Preparation, microstructure and property of carbonated artificial steel slag aggregate used in concrete. *Cem. Concr Compos.* **113**, 103715. https://doi.org/10.1016/j.cemconcomp.2020.103715 (2020).
38. Zhang, T., Hou, J. K. & Gao, S. Axial mechanical and environmental properties of CFRP-confined coal gangue sand concrete. *J. Build. Eng.* **108**, 112785. https://doi.org/10.1016/j.jobe.2025.112785 (2025).
39. Buettner, N., Iyacu, G., Poggetto, D., Akono, A. T. & G.D. & Critical role of carbon nanofibers in boosting C-S-H density and fracture toughness in fine recycled aggregate concrete. *Sci. Rep.* **15**, 27544. https://doi.org/10.1038/s41598-025-11530-9 (2025).
40. Irshidat, M. R., Al-Nuaimi, N. & Rabie, M. Microstructure and mechanical behavior of cementitious composites with multi-scale additives. *Adv. Concr Constru.* **11** (2), 163–171. https://doi.org/10.12989/ACC.2021.11.2.163 (2021).
41. Sun, K. K. et al. Probing the micromechanical properties of seawater-mixed alkali-activated slag: insights from nano-indentation and EDX. *Cem. Concr Compos.* **164**, 106301. https://doi.org/10.1016/j.cemconcomp.2025.106301 (2025).
42. Lin, K. L. & Lin, C. Y. Hydration characteristics of waste sludge Ash utilized as Raw cement material. *Cem. Concr Res.* **35** (10), 1999–2007. https://doi.org/10.1016/j.cemconres.2005.06.008 (2005).
43. Yang, R. & Buenfeld, N. R. Binary segmentation of aggregate in SEM image analysis of concrete. *Cem. Concr Res.* **31** (3), 437–441. https://doi.org/10.1016/S0008-8846(00)00493-2 (2001).
44. Zhao, X. Y. et al. Mix proportion and microscopic characterization of coal-based solid waste backfill material based on response surface methodology and multi-objective decision-making. *Sci. Rep.* **14**, 5672. https://doi.org/10.1038/s41598-024-56028-y (2024).
45. Wang, C. B. et al. Exploring calcined coal gangue fines as the total substitute of fly Ash in the production of alkali-activated slag/fly Ash materials. *Case Stud. Constr. Mater.* **17**, e01332. https://doi.org/10.1016/j.cscm.2022.e01332 (2022).
46. Xu, C. Y. et al. Structure Characteristics and combustion kinetics of the co-pyrolytic Char of rice straw and coal gangue. *Sci. Rep.* **14**, 16320. https://doi.org/10.1038/s41598-024-67378-y (2024).
47. Zhu, H. G. et al. Study on compressive strength and Frost resistance of coal gangue fine Aggregate-Slag Cement-based concrete. *Mater. Rev.* **35** (22), 22085–22091. https://doi.org/10.11896/cldb.20080019 (2021).
48. Li, Y. G., Zhang, H. M., Liu, G. X., Hu, D. W. & Ma, X. R. Multi-scale study on mechanical property and strength prediction of aeolian sand concrete. *Constr. Build. Mater.* **247**, 118538. https://doi.org/10.1016/j.conbuildmat.2020.118538 (2020).
49. Huang, J. D. et al. Influence of porosity and cement grade on concrete mechanical properties. *Adv. Concr Constru.* **10** (5), 393–402. https://doi.org/10.12989/ACC.2020.10.5.393 (2020).
50. Heijden, D. V. G., Pel, L. & Adan, O. Fire spalling of concrete, as studied by NMR. *Cem. Concr Res.* **42** (2), 265–271. https://doi.org/10.1016/j.cemconres.2011.09.014 (2012).
51. Pop, A., Badea, C. & Ardelean, I. The effect of different superplasticizers and water-to-cement ratios on the hydration of Gray cement using T_2-NMR. *Appl. Magn. Reson.* **44** (10), 1223–1234. https://doi.org/10.1007/s00723-013-0475-5 (2013).
52. Tu, Q. C., Xia, Q. H. & Bai, Y. H. Preparation of coal gangue foam concrete modified by nanomaterials: physical properties, pore structure, and electromagnetic properties. *Case Stud. Constr. Mater.* **21**, e03603. https://doi.org/10.1016/j.cscm.2024.e03603 (2024).
53. Wu, Z. W. Discussion on the recent development direction of concrete science and technology. *J. Chin. Ceram. Soc.* **7** (03), 262–270. https://doi.org/10.14062/j.issn.0454-5648.1979.03.010 (1979).
54. Sun, K. K. et al. Effect of nano-SiO2 on the efflorescence of an alkali-activated Metakaolin mortar. *Constr. Build. Mater.* **253**, 118952. https://doi.org/10.1016/j.conbuildmat.2020.118952 (2020).

Acknowledgements

This work was supported by the National Natural Science Foundation of China with Grant No.s of 52268047, 51868075, 12302490 and 52368041, Yulin Science and Technology Bureau of Shaanxi Province with a Grant No. of 2023-CXY-145, Yulin High-tech Zone Science and Technology Bureau with a Grant No. of YGXKG-2023-106.

Author contributions

D.W. Hu Writing-original alraft, Conceptualization, MethodsD.Y. Lou Writing-original alraft, Data curation, ExperimentY.G. Li Writing-original alraft, Conceptualization, Funding acquisitionP. He Investigation, Experiment, Writing-review & editingX.L. Ma Writing-review & editing, Funding acquisition, InvestigationY.N. Kang Data analysis, Investigation, Methods F. Wei Funding acquisition, Methods, Writing-review & editingAll authors reviewed the manuscript.

Declarations

Competing interests
The authors declare no competing interests.

Additional information
Correspondence and requests for materials should be addressed to Y.L.

Reprints and permissions information is available at www.nature.com/reprints.

Publisher's note Springer Nature remains neutral with regard to jurisdictional claims in published maps and institutional affiliations.